ChemComm

COMMUNICATION

View Article Online
View Journal | View Issue

Cite this: *Chem. Commun.*, 2022, **58**, 9246

Received 20th June 2022,
Accepted 19th July 2022

DOI: 10.1039/d2cc03456e

rsc.li/chemcomm

Anisotropic and hyperbranched InP nanocrystals *via* chemical transformation of *in situ* produced In_2O_3†

Shuai Chen and Andreas Riedinger *

We synthesized indium phosphide (InP) nanoparticles of different shapes and sizes, utilizing triphenyl phosphite (TPOP) as the phosphorus source. We show that this reaction proceeds *via* the formation of *in situ* formed In_2O_3 nanoparticles followed by subsequent transformation with triphenyl TPOP acting as the phosphorus source. Our findings open up new synthetic possibilities utilizing a cost-effective, non-pyrophoric and non-toxic phosphorus precursor. The large surface area of hyperbranched InP NCs might be ideally suited for surface-driven processes such as catalysis and energy storage.

The synthesis of colloidal nanocrystals (NCs) with regular and controllable morphology and size is at the core of nanomaterials research.[1–3] Many synthesis approaches have been developed to produce high-quality nanoparticles, nanorods, nanowires, or other nanostructures for metals, semiconductors, and oxides.[4–7] The control over morphology and functionalization in preparation and synthesis are an important part of the development of nanotechnology and are the basis for exploring the properties of nanostructures and their applications.[8–10]

Indium phosphide (InP) is one of the most widely studied III–V compound semiconductors nanocrystals in colloidal form.

InP nanowires (NWs) have attracted considerable interest due to their versatility in electronics and optoelectronics.[11–14] And InP quantum dots are drawing a large interest as a potentially less toxic material for lighting applications and electrochemical reduction of CO_2.[15–17] Potentially, there are still many different shapes of InP NCs waiting for their discovery.

Until now, various types of P precursors have been reported to synthesize InP NCs, such as single-source precursor ($In(PBu^t_2)_3$),[18] magic sized clusters (MSCs),[19] elemental phosphorus precursor,[20] trioctylphosphine (TOP),[21] PH_3 gas,[22] aminophosphine,[23] metal phosphorus (Na_3P),[24] and most widely, tris(trimethylsilyl) phosphine $P(SiMe_3)_3$.[25] However, many of these P precursors, in particular $P(SiMe_3)_3$, are air and water sensitive, hazardous, and/or expensive. Therefore, alternative, safer and cheaper P precursors are very desirable (Scheme 1).

Among various phosphites, triphenyl phosphite (TPOP) would be the most effective P precursor for InP synthesis, since three benzene rings would stabilize the partial charges for In-P monomer formation.[27] Interestingly, TPOP is reported as an effective phosphorus source for synthesizing various metal phosphide nanocrystals such as Ni_2P, MoP, Co_2P, Fe_2P, and Cu_3P.[26] Recently, Lee *et al.* used TPOP to synthesize bulk InP.[27] A black powder appeared after the purification process but was not be dispersible in solvents. This is a promising method because TPOP can form InP phases, it is a cheap and non-pyrophoric, non-toxic chemical. However, so far, no control over size and shape with TPOP as a precursor for InP nanomaterials has been reported.

Here, we show how this can be achieved by choosing the right synthetic conditions in the reaction between indium chlorides and carboxylates and TPOP in the presence hexadecylamine (HDA) in octadecene (ODE), in order to yield InP NCs with control over size and shape. We show that by changing the temperature, we mainly gain control over the shape that spans from wires to tetrahedrons to hyperbranched NCs. The size of InP NCs could be controlled by hot injection of TPOP. We also

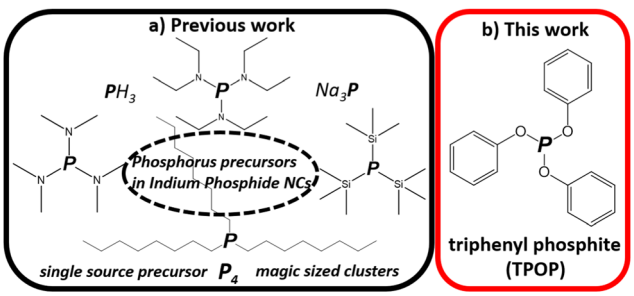

Scheme 1 Phosphorus precursors in synthesis of indium phosphide NCs.

Max Planck Institute for Polymer Research, Ackermannweg 10, 55128, Mainz, Germany. E-mail: riedinger@mpip-mainz.mpg.de

† Electronic supplementary information (ESI) available. See DOI: https://doi.org/10.1039/d2cc03456e

investigate the formation of InP. We find that In_2O_3 is formed first, and converted to InP upon addition TPOP.

Here, the InP NCs were prepared by a one-pot reaction of indium chloride and indium acetate in a mixture of TPOP as a phosphorus source and HDA as a stabilizer in ODE as solvent. In a typical synthesis, 0.5 mmol of $In(ac)_3$, 0.5 mmol $InCl_3$, 5 mmol HDA, 1.5 mL TPOP were mixed with 15 mL ODE. The mixture was heated up to 150 °C in 15 minutes under an argon atmosphere and kept at 150 °C for 60 minutes. Then, the mixture was heated to a higher temperature (230–320 °C) within several minutes and kept at this temperature for 30 min. For experimental details, please see the ESI.† Our experiments found that the molar ratio of the $InCl_3$: $In(ac)_3$ was a key factor that affects the formation of the indium phosphide NCs. With only $InCl_3$ or $In(ac)_3$ as In precursor, the color of the solution did not change even during prolonged heat treatment, and no product could be precipitated from the reaction solution (Fig. S10, ESI†). However, InP particles formed when we utilized mixtures of $In(ac)_3$ and $InCl_3$ as the In precursor. Only a molar ratio of 1 : 1 of $In(ac)_3$: $InCl_3$ resulted in the formation of regular InP NCs.

The temperature dependence of the nanoparticle size and shape was investigated for a range of 230–320 °C. In these experiments, all other variables remained constant. The transmission electron microscopy (TEM) images reveal the differently shaped nanomaterials resulting from varying the temperatures (see Fig. 1). The temperature affects the nanocrystal's size and shape, ranging from nanowires to tetrahedrons and hyperbranched NCs. As powder X-ray diffraction (PXRD) revealed, all products displayed a cubic InP crystal phase in the space group $F\bar{4}3m$, with $a = b = c = 0.587$ nm (see Fig. 1). The appreciable diffraction peaks at $2\Theta = 26.34$, 30.48, 43.58 and 51.78 are assigned to the (111), (200), (220) and (311) planes of InP (PDF#65-0233), respectively.

We used the one-pot heating-up method to track the transient reaction process at different temperatures (230 °C, 240 °C, 250 °C, 260 °C, 280 °C, and 300 °C) to see the transient change of the morphologies and phases of the product. As we can see from the result (Fig. S1, ESI†), InP forms at 230 °C and bigger particles are formed later (*i.e.* at higher temperatures) during heat-up process. Furthermore, we investigated the impact of hot injection of additional TPOP after formation of InP by heat-up reaction scheme. At room temperature, we added $InCl_3$, $In(ac)_3$, HDA, TPOP, and ODE to the flask. Since the color of the mixture had already become intensely dark at 270 °C, we injected different amounts of TPOP into the reaction mixture. Fig. 2 displays representative TEM micrographs and the PXRD patterns of the InP NCs produced following this procedure.

It is interesting to note that the NCs size increased when decreasing the amount of TPOP. For example, when we injected 1 mL of TPOP into the solution, we were able to synthesize the biggest hyperbranched NCs with a diameter around 160 nm (Fig. 2e). Fig. 2a–d show TEM images of InP NCs with sizes of around 20 nm, 70 nm, 80 nm, and 120 nm, which were synthesized at injection amounts of 3 mL, 2.5 mL, 2 mL, 1.5 mL, and 1 mL of TPOP, respectively. For more TEM micrographs, please see S2–S6 (ESI†). PXRD patterns reveal that the NCs are all in the cubic InP phase, with $F\bar{4}3m$ space group (Fig. 2f). In the literature, acetic acid was used to tune the shape of PbS nanoparticles from quasi-spherical particles *via* octahedrons to six-armed stars.[29] While we did not see any clear morphological changes induced by acetic acid, we found that spiking the reaction mixture with varying amounts of acetic acid smaller tetrahedron-shaped InP nanoparticles with sizes in the range of 10–20 nm can be obtained (Fig. S7, ESI†).

To shed some light on the InP nanomaterial formation, we monitored the formation of eventual intermediate products during a typical synthesis, as summarized in Fig. 3. At first,

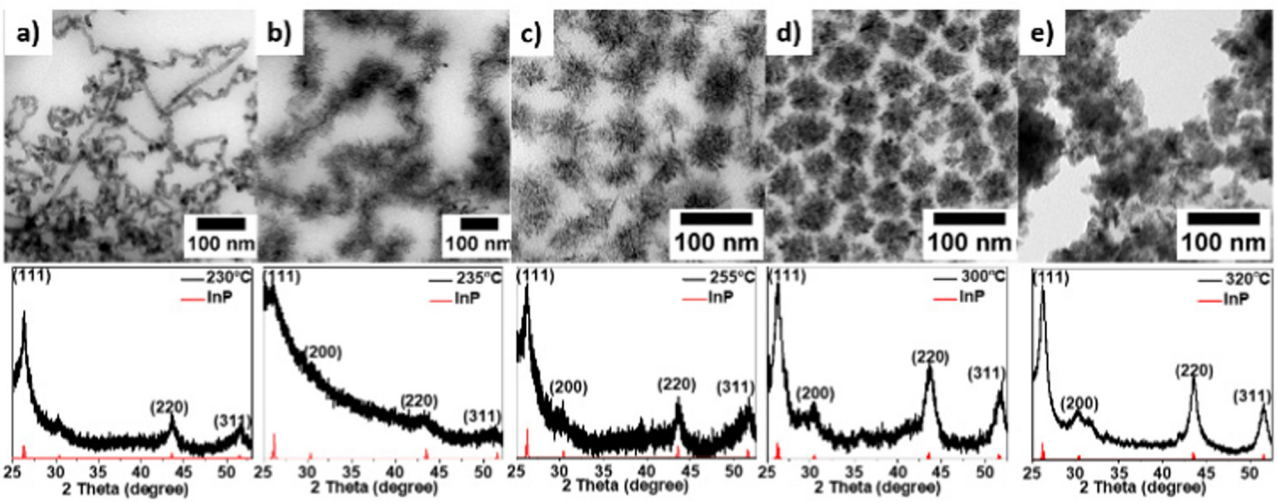

Fig. 1 TEM images and PXRD patterns of indium phosphide NCs synthesized at different temperatures, ranging from 230 °C to 320 °C. At lower temperatures, InP wires are formed (a). Increasing the temperature leads frist to branching on the wires (b), then to hyperbranched spherical InP nanoparticles (c). Increasing the temperature above 300 °C leads to a reduced length of the branches (d) and finally, NCs are sintered together into large aggregates (e).

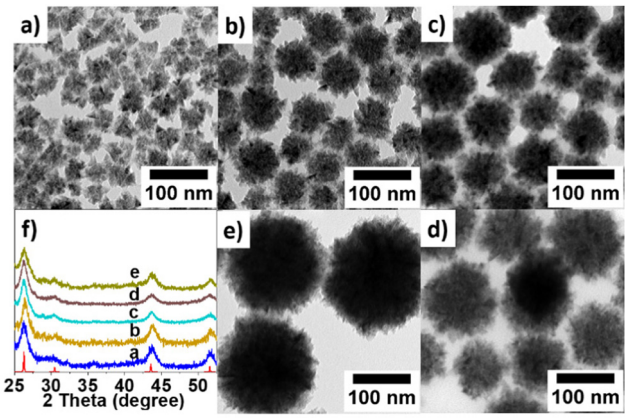

Fig. 2 TEM images and PXRD of InP NCs synthesized with different amounts of TPOP injected at 270 °C. (a) 3 mL TPOP; (b) 2.5 mL TPOP; (c) 2 mL TPOP; (d) 1.5 mL TPOP; (e) 1 mL TPOP.

we added $InCl_3$, $In(ac)_3$, HDA, and ODE to the reaction flask at heated the mixture to 150 °C for 60 min. Then we injected the TPOP at 270 °C. Aliquots were taken before and after TPOP addition and analyzed by TEM and PXRD. Interestingly, ~60 nm-sized InP hyper branch NCs (Fig. 3b) formed from ~20 nm-sized In_2O_3 NCs (Fig. 3c). During the heating process, we collected aliquots at 150 °C (Fig. S8a, ESI†) and 270 °C (Fig. S8b, ESI†) before TPOP was added. These experiments demonstrate, that In_2O_3 is formed already after 60 min at 150 °C and still present at 270 °C, as the PXRD pattern was found to match the reference pattern of In_2O_3 (Fig. 3a). No additional peaks were observed, suggesting that few or no crystalline impurities were present. Then we injected the TPOP at 270 °C, and the PXRD patterns for samples collected after 5, 10, and 60 min of reaction at 270 °C showed the progressive transformation of the In_2O_3 NCs to InP NCs. The planes on these NPs (generally (111) or (220)) are readily available for P diffusion.[30] After 33 min, the complete transformation of the In_2O_3 NCs into hyperbranched InP NCs was confirmed by PXRD and TEM (Fig. 3). Based on this interesting observation, commercial In_2O_3 was used to do the reaction under the same conditions, but we could not yield InP NCs (Fig. S9, ESI†). This hints that the transformation from In_2O_3 to InP only works when the oxide NCs are produced from $In(ac)_3$ and $InCl_3$. We speculate that the halide on the oxide NCs' surface plays an important role in this reaction. We also tested $InBr_3$ and InI_3 in the synthesis to evaluate the role of halides. We found that they also formed the InP. Hence also bromides and iodides can facility the formation of InP, even though the sizes of the resulting NCs were quite different (Fig. S11, ESI†). For example, the halide ion influence the formation of nickel nanoparticles and their conversion into hollow nickel phosphide.[31]

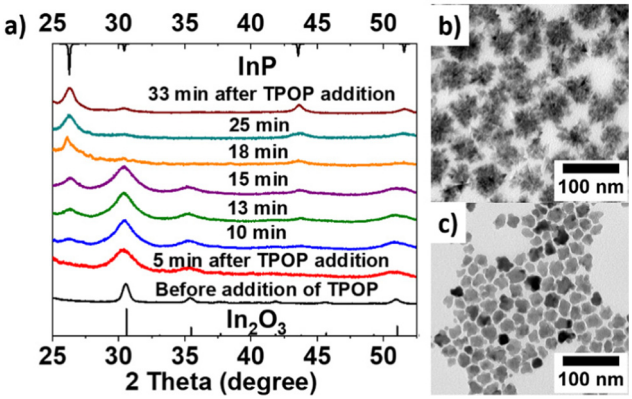

Fig. 3 Illustration of In_2O_3 to form InP. (a) PXRD with before and after addition of TPOP; (b) TEM of InP NCs; (c) TEM of In_2O_3 NCs at 270 °C before addition of TPOP.

The transformation of metal oxides to metal phosphides is known for a variety of nanomaterials, yet not for InP. Brock *et al.*[28] studied the NiO nanoparticles that enable their transformation into Ni_2P phosphides by solution-phase reaction with trioctyl phosphine (TOP) at temperatures of 385 °C. Sun *et al.*[30] reported that bimetallic phosphides, Co–Fe–P could be obtained by the reaction between Co–Fe–O nanoparticles and TOP at high temperature for 12 h. Surprisingly, we were able to yield InP NCs at lower temperatures in around 2 hours.

In summary, this work presents a facile approach to nanostructured InP *via* a high-temperature (230–320 °C) reaction of indium chloride and indium acetate with TPOP. In the synthesis, the co-presence of acetate and chloride is necessary for the formation of InP NCs and facilitates the anisotropic growth of InP into either wires, tetrahedrons, or hyperbranched NCs. The size of the NCs is controlled by the amount of (hot injected) TPOP. Our experiments revealed that the formation of InP proceeds *via* the chemical transformation of *in situ* produced In_2O_3 NCs. Our approach provides a new approach to indium phosphides with control of morphology and size. This new approach to anisotropic and hyperbranched InP nanomaterials is especially interesting for applications that require large surface areas, such as catalysis and energy storage applications.

We thank Michael Steiert and Christoph Sieber for XRD measurements, and Prof. Mischa Bonn for the fruitful discussions. Open Access funding provided by the Max Planck Society. Shuai Chen acknowledge fellowship support from China Scholarship Council (CSC).

Conflicts of interest

There are no conflicts to declare.

Notes and references

1 A. P. Alivisatos, *Chem. Rev.*, 1996, **271**, 933–937.
2 M. A. El-Sayed, *Acc. Chem. Res.*, 2004, **37**, 326–333.
3 D. V. Talapin, J. S. Lee, M. V. Kovalenko and E. V. Shevchenko, *Chem. Rev.*, 2010, **110**, 389–458.
4 P. Reiss, M. Carriére, C. Lincheneau, L. Vaure and S. Tamang, *Chem. Rev.*, 2016, **116**, 10731–10819.
5 Y. Chen, Z. X. Fan, Z. C. Zhang, W. X. Niu, C. L. Li, N. L. Yang, B. Chen and H. Zhang, *Chem. Rev.*, 2018, **118**, 6409–6455.
6 J. Tang and E. H. Sargent, *Adv. Mater.*, 2011, **23**, 12–29.
7 Y. P. Du and G. Xie, *CrystEngComm*, 2011, **13**, 437–439.
8 J. Y. Mao, X. Q. Cao, J. W. Zhen, H. L. Shao, H. W. Gu, J. M. Lu and J. Y. Ying, *J. Mater. Chem.*, 2011, **21**, 11478–11481.

9 H. J. Wang, H. Y. Jeong, M. Imura, L. Wang, L. Radhakrishnan, N. Fujita, T. Castle, O. Terasaki and Y. Yamauchi, *J. Am. Chem. Soc.*, 2011, **133**, 14526–14529.
10 D. Astruc, *J. Am. Chem. Soc.*, 2020, **120**, 461–463.
11 X. Duan, Y. Huang, Y. Cui, J. Wang and C. M. Lieber, *Nature*, 2001, **409**, 66–69.
12 J. Wang, M. S. Gudiksen, X. Duan, Y. Cui and C. M. Lieber, *Science*, 2001, **293**, 1455–1457.
13 F. D. Wang, H. Yu, J. B. Li, Q. L. Hang, D. Zemlyanov, P. C. Gibbons, L. W. Wang, D. B. Janes and W. E. Buhro, *J. Am. Chem. Soc.*, 2007, **129**, 14327–14335.
14 J. M. Sun, Y. X. Yin, M. M. Han, Z. X. Yang, C. Y. Lan, L. Z. Liu, Y. Wang, N. Han, L. F. Shen, X. L. Wu and J. C. Ho, *ACS Nano*, 2018, **12**, 10410–10418.
15 B. Chen, D. Y. Li and F. Wang, *Small*, 2020, **16**, 2002454.
16 J. J. Calvin, J. K. Swabeck, A. B. Sedlak, Y. W. Kim, E. Jang and A. P. Alivisatos, *J. Am. Chem. Soc.*, 2020, **142**, 18897–18906.
17 I. Grigioni, L. K. Sagar, Y. C. Li, G. Lee, Y. Yan, K. Bertens, R. K. Miao, X. Wang, J. Abed, D. H. Won, F. P. G. Arquer, A. H. Ip, D. Sinton and E. H. Sargent, *ACS Energy Lett.*, 2021, **6**, 79–84.
18 M. Green and P. O'Brien, *Chem. Commun.*, 1998, 2459–2460.
19 M. R. Friedfeld, J. L. Stein and B. M. Cossairt, *Inorg. Chem.*, 2017, **56**, 8689–8697.
20 T. D. T. Ung, T. T. H. Tran, Q. L. Nguyen and P. Reiss, *Mater. Chem. Phys.*, 2008, **112**, 1120–1123.
21 P. Ramasamy, N. Kim, Y. S. Kang, O. Ramirez and J. S. Lee., *Chem. Mater.*, 2017, **29**, 6893–6899.
22 F. Zan and J. C. Ren, *J. Mater. Chem.*, 2012, **22**, 1794–1799.
23 M. E. Mundy, D. Ung, N. L. Lai, E. P. Jahrman, G. T. Seidler and B. M. Cossairt, *Chem. Mater.*, 2018, **30**, 5373–5379.
24 K. W. Jun, P. K. Khanna, K. B. Hong, J. O. Baeg and Y. D. Suh, *Mater. Chem. Phys.*, 2006, **96**, 494–497.
25 P. Ramasamy, N. Kim, Y. S. Kang, O. Ramirez and J. S. Lee, *Chem. Mater.*, 2017, **29**, 6893–6899.
26 J. F. Liu, M. Meyns, T. Zhang, J. Arbiol, A. Cabot and A. Shavel, *Chem. Mater.*, 2018, **30**, 1799–1807.
27 D. Lee, S. Koh, D. E. Yoon, S. Lee, W. D. Kim, D. Kim, W. K. Bae, J. Lim and D. C. Lee, *Korean J. Chem. Eng.*, 2019, **36**, 1518–1526.
28 E. Muthuswamy and S. L. Brock, *J. Am. Chem. Soc.*, 2010, **132**, 15849–15851.
29 F. Gerdes, M. Volkmann, C. Schliehe, T. Bielewicz and C. Klinke, *Z. Phys. Chem.*, 2015, **229**, 139–151.
30 A. M. Garcia, H. Y. Zhu, Y. S. Yu, Q. Li, L. Zhou, D. Su, M. J. Kramer and S. H. Sun, *Angew. Chem., Int. Ed.*, 2015, **54**, 9642–9645.
31 R. Himstedt, D. Hinrichs, J. Sann, A. Weller, G. Steinhauserd and D. Dorfs, *Nanoscale*, 2019, **11**, 15104–15111.